

JGR Space Physics

RESEARCH ARTICLE

10.1029/2019JA027143

Key Points:

- The maximum magnetic shear model predicts a stationary reconnection X-line in a region where the magnetosheath flow is likely to be super-Alfvénic
- Observations of transmitted and return beams in the low latitude boundary layer for some restrictive conditions show that there is a quasi-stationary reconnection X-line near the predicted location
- Alternatively, there could be multiple X-lines formed at the magnetopause and these observations place constraints on the formation frequency and motion of multiple X-lines

Correspondence to:

S. A. Fuselier,
 stephen.fuselier@swri.org

Citation:

Fuselier, S. A., Trattner, K. J., Petrinec, S. M., Pritchard, K. R., Burch, J. L., Cassak, P. A., et al. (2019). Stationarity of the reconnection X-line at Earth's magnetopause for southward IMF. *Journal of Geophysical Research: Space Physics*, 124, 8524–8534. <https://doi.org/10.1029/2019JA027143>

Received 9 JUL 2019

Accepted 27 SEP 2019

Accepted article online 17 OCT 2019

Published online 7 NOV 2019

Stationarity of the Reconnection X-Line at Earth's Magnetopause for Southward IMF

S. A. Fuselier^{1,2} , K. J. Trattner³ , S. M. Petrinec⁴ , K. R. Pritchard^{2,1} , J. L. Burch¹ , P. A. Cassak⁵ , B. L. Giles⁶ , B. Lavraud⁷ , and R. J. Strangeway⁸ 

¹Southwest Research Institute, San Antonio, TX, USA, ²Department of Physics and Astronomy, University of Texas at San Antonio, San Antonio, TX, USA, ³Laboratory for Atmospheric and Space Physics, University of Colorado Boulder, Boulder, CO, USA, ⁴Lockheed Martin Advanced Technology Center, Palo Alto, CA, USA, ⁵Department of Physics and Astronomy, West Virginia University, Morgantown, WV, USA, ⁶NASA Goddard Space Flight Center, Greenbelt, MD, USA, ⁷Institut de Recherche en Astrophysique et Planétologie, Université de Toulouse, CNRS, UPS, CNES, Toulouse, France, ⁸Department of Earth and Space Sciences, University of California, Los Angeles, CA, USA

Abstract When the interplanetary magnetic field (IMF) is southward and has a substantial Y component, reconnection at the magnetopause occurs at low latitudes. Under these conditions, the maximum magnetic shear model for the reconnection X-line at the magnetopause predicts a continuous X-line stretching from the dawn to dusk terminators. During the solstices, the X-line is not at the subsolar point and may be located in a region where the magnetosheath bulk flow is super-Alfvénic. For a fixed IMF direction, the maximum shear model also predicts a stationary X-line. In response to IMF clock angle changes on the timescale of minutes, the X-line moves on the same timescale. The stationarity of the reconnection X-line is testable observationally under certain, restrictive conditions. This stationarity is tested using observations from the Magnetospheric Multiscale mission. For two events, the distance from the Magnetospheric Multiscale spacecraft to the X-line is constant over several minutes (within relatively large error bars) and the X-line is also near the location predicted by the maximum magnetic shear model. Thus, the reconnection X-line at the magnetopause appears to be quasi-stationary for constant IMF clock angle. These observations also place constraints on the formation and motion of multiple X-lines at the magnetopause.

1. Introduction

Magnetic reconnection occurs at the Earth's magnetopause for all orientations of the interplanetary magnetic field (IMF). For southward IMF, reconnection occurs equatorward of the Earth's magnetospheric cusps at the low-latitude magnetopause. This reconnection occurs between magnetosheath and magnetospheric fields along continuous reconnection X-lines. The reconnection X-line is envisioned conveniently as a ribbon stretching across a large part of the dayside magnetopause (Fuselier et al., 2016).

This ribbon is very thin. In the electron diffusion region, that is, in the heart of the X-line where the magnetosheath and magnetospheric field lines break and reconnect, the ribbon thickness is of the order of an electron inertial length. At the magnetopause, this thickness is of the order of 2 km (e.g., Fuselier & Lewis, 2011; Hesse, 2006). The ribbon is also very narrow. The width of the electron diffusion region is of the order of 10 electron inertial lengths, which, at the magnetopause is of the order of 20 km. Compared to its thickness and width, the ribbon is very, very long. There is observational evidence that reconnection X-lines are many tens of thousands of km, or equivalently, many Earth radii (R_E) long (e.g., Fuselier et al., 2002; Petrinec & Fuselier, 2003; Petrinec et al., 2003; Phan et al., 2000; Trattner et al., 2007a, 2007b).

Depending on the relative strengths of the $IMF|B_y|$ and $|B_z|$ components and the location on the magnetopause, the shear angle between the magnetosheath and magnetospheric magnetic fields at the reconnection X-line is either 180° (antiparallel reconnection) or $<180^\circ$ (component, or guide field reconnection). One empirical model that has been very successful in predicting where reconnection X-lines occur and where there is antiparallel and component reconnection is the maximum shear reconnection model (Trattner et al., 2007a, 2007b). This model was developed from a large number of measurements in the Earth's magnetospheric cusps and has been tested successfully using in situ observations at the Earth's magnetopause (Dunlop et al., 2011; Fuselier et al., 2011; Petrinec et al., 2016; Trattner et al., 2012; Trattner et al., 2017) and using energetic neutral atom observations to remotely image the magnetospheric cusps (Petrinec et al., 2011). The

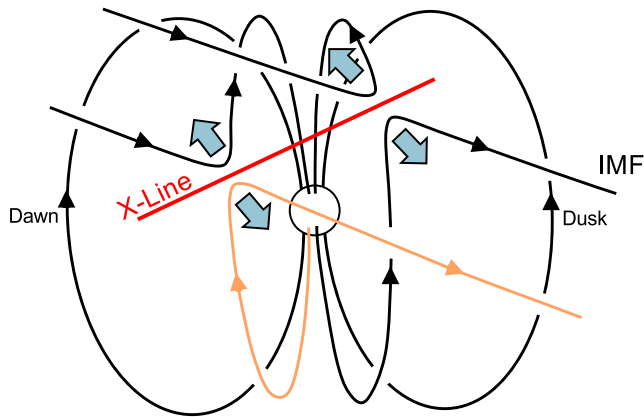


Figure 1. Schematic view of the component reconnection X-line that forms when the interplanetary magnetic field (IMF) is southward, $|+B_Y| \geq |-B_Z|$, and the time of year is around the northern hemisphere winter solstice. The view is from the Sun. Reconnected field lines convect away from the component X-line under the tension of the IMF convection. The duskward convection of the orange field line in the low-latitude boundary layer (LLBL) is opposed to the dawnward magnetosheath flow. These flow reversals are unique to component reconnection at the magnetopause. If this duskward convection is slow enough, then high-velocity ions that enter the LLBL near the reconnection site have time to propagate along the field line to the ionosphere, mirror, and return to the LLBL. This figure is adapted from Gosling et al. (1990).

model was used successfully to predict the reconnection diffusion region encounters by the Magnetospheric Multiscale (MMS) mission (Fuselier et al., 2016).

The maximum shear model of the reconnection line location predicts that there is a combination of component and antiparallel reconnection at the magnetopause when the IMF is southward and $|+B_Y| \geq |-B_Z|$. Furthermore, there is a seasonal effect that moves the component part of the reconnection X-line away from the subsolar region. The result is a reconnection X-line configuration similar to that shown schematically in Figure 1. It shows the magnetopause location of a component part of the reconnection X-line for $+B_Y \sim |-B_Z|$ near the December solstice. The component X-line extends over a large fraction of the dayside magnetopause and is offset from the subsolar region because of the time of the year (see, Trattner et al., 2007b). The tilt of the X-line and its offset from the subsolar region have important consequences for the ion reconnection flow jets in the low-latitude boundary layer (LLBL). In particular, the flow jet associated with the reconnected field line in orange in Figure 1 is in the dusk direction, which is opposite the dawnward magnetosheath flow. These “plasma flow reversal events” (Gosling et al., 1990) were recognized as unique to component reconnection at the magnetopause and, indeed, Figure 1 is a modified version of Figure 1 in Gosling et al. (1990).

During the solstices, the component reconnection X-line is sufficiently far off the subsolar point such that all or substantial parts of it may be

located in regions where the magnetosheath bulk flow velocity at the magnetopause is super-Alfvénic. Petrinec et al. (2003) investigated the sub-sonic to super-sonic transition for northward IMF conditions. They used a relatively simple model of the magnetosheath flow past the magnetopause; however, their results are applicable to a wider range of IMF orientations. In their model, the magnetosheath flow becomes super-Alfvénic of the order of $5 R_E$ away from the subsolar point in either the Y or Z directions. Thus, the component reconnection X-line is likely in a super-Alfvénic flow regime when $|+B_Y| \geq |-B_Z|$ near the December or June solstices. The magnetosheath flow radially away from the subsolar point is approximately perpendicular to this reconnection X-line.

These results raise the question whether the reconnection X-line location remains steady in such a flow regime, or if the X-line propagates tailward at the bulk flow speed of the magnetosheath plasma (so that the shear flow across the X-line is small) or, alternatively at approximately the Alfvén speed. In the maximum shear model, the reconnection line moves along the magnetopause in response to changes in the IMF, but otherwise it is stationary. Magnetopause crossings near and in the electron diffusion region by the MMS spacecraft show that the reconnection X-line is in motion (e.g., Burch et al., 2016; Cassak et al., 2017; Lavraud et al., 2016)). The MMS spacecraft at the magnetopause are moving at 1-2 km/s while the magnetopause moves radially in and out at ~ 20 km/s. Thus, the spacecraft cross the magnetopause because the boundary sweeps over the relatively stationary spacecraft. The reconnection diffusion region also sweeps past the spacecraft at speeds tangential to the magnetopause that are often much greater than the in and out motion of the magnetopause. Reconnection X-line speeds of ~ 100 km/s are not uncommon (Burch et al., 2016; Pritchard et al., 2019). However, the spacecraft usually reside in the diffusion region and associated magnetopause boundary layers for a few seconds. These brief diffusion region encounters are not sufficient to determine if the reconnection X-line motion along the magnetopause is sustained for a significant period of time (e.g., many minutes).

Up to this point, the discussion has focused on a single, primary X-line. There is also observational evidence of multiple, secondary X-lines at the magnetopause (e.g., Fuselier et al., 2011; Hasegawa et al., 2010; Pu et al., 2005; Trattner et al., 2012; Vines et al., 2017; Wang et al., 2007; Wilder et al., 2014;). Observations discussed in sections 3 and 4 place constraints on the formation and motion of multiple X-lines. These constraints are presented in the interpretation section.

The purpose of this paper is to investigate the location and possible motion of the X-line on a timescale longer than several seconds. Two magnetopause crossings by the MMS spacecraft are used in this investigation. These two crossings occurred near the December solstice when IMF $+B_Y \geq |-B_Z|$ (i.e., the IMF conditions and time of year discussed above). For these two crossings, it is shown that the MMS observations are consistent with a quasi-stationary, component reconnection X-line and is likely located in a super-Alfvénic flow regime. The term quasi-stationary is defined here as remaining at a fixed distance from the spacecraft (within some uncertainty that is defined from the observations) for several minutes. While the X-line may move around this fixed distance within this fairly large uncertainty, it does not appear to move in a consistent manner away from (or toward) the spacecraft. Section 2 describes the instrumentation and method used to determine the stationarity of the X-line. Section 3 and 4 describe the observations from the first and second magnetopause crossings, respectively. Section 5 describes the interpretation of the observations and the conclusions. The interpretation section is divided into two sub-sections in order to discuss separately the single X-line and multiple X-line interpretations.

2. Instrumentation and Method

Observations in this paper are from the MMS spacecraft at the magnetopause. Single spacecraft observations are sufficient for this study and MMS3 observations are used here. The Fast Plasma Investigation/Dual Electron Spectrometer (FPI/DES; Pollock et al., 2016) observations are used to help identify the plasma regions encountered by the spacecraft. Hot Plasma Composition Analyzer (HPCA; Young et al., 2016) and magnetic field (MAG; Russell et al., 2016) observations are used to determine pitch angle distributions in the LLBL. Finally, WIND observations (Lepping et al., 1995; Ogilvie et al., 1995) are used to determine the upstream conditions for the magnetopause encounters.

The distance to the reconnection site is determined by employing a proven technique that utilizes ion populations observed in reconnection boundary layers such as the plasma sheet boundary layer, LLBL or magnetospheric cusps (e.g., Fuselier et al., 1992; Fuselier et al., 2000; Onsager et al., 1990; Onsager & Fuselier, 1994; Phillips et al., 1993; Trattner et al., 2007a, 2007b). In these boundary layers, there is a time-of-flight or velocity filter effect that produces populations with distinct low-speed cutoff velocities. Considering the orange field line in Figure 1, if the convection of the reconnected field line from the X-line is slow enough, then a spacecraft at the subsolar point in the LLBL observes two ion populations propagating in opposite directions along the magnetic field. This requirement on the field line convection speed is explained further in the observations section. The first population, propagating antiparallel to the orange magnetic field line, is the magnetosheath population that entered the magnetosphere on open field lines poleward of the spacecraft. The second population, propagating parallel to the orange magnetic field line, is the magnetosheath population that entered the magnetosphere, propagated to the ionosphere, mirrored, and returned to the spacecraft. The low-speed cutoffs of both the entering and mirrored populations represent the particles arriving at the spacecraft from near the reconnection site. Since these particles left the reconnection site at the same time, the propagation times from the site to the spacecraft are equal. The two equations that describe the distance, velocity, and common propagation time of the two populations are solved for the distance to the reconnection site (see, Onsager et al., 1990) giving:

$$X_R = X_M \frac{2V_E}{(V_M - V_E)} \quad (1)$$

In equation (1), X_R is the distance from the spacecraft to the reconnection site, X_M is the distance from the spacecraft to the mirror point in the ionosphere, V_E is the cutoff speed along the magnetic field of the earthward propagating population, and V_M is the cutoff speed along the magnetic field of the return, or mirrored population. In practice, X_M is determined from a model magnetospheric field like the Tsyganenko model field (Tsyganenko, 1995) used here.

3. Observations: 7 December 2016 Magnetopause Crossing

The MMS3 spacecraft crossed the magnetopause several times on 7 December 2016 starting at approximately 0519 UT. The spacecraft was very near the subsolar point. The IMF clock angle was 125° and B_X was relatively small compared to the total field strength ($|B_X|/|B| = 0.4$).

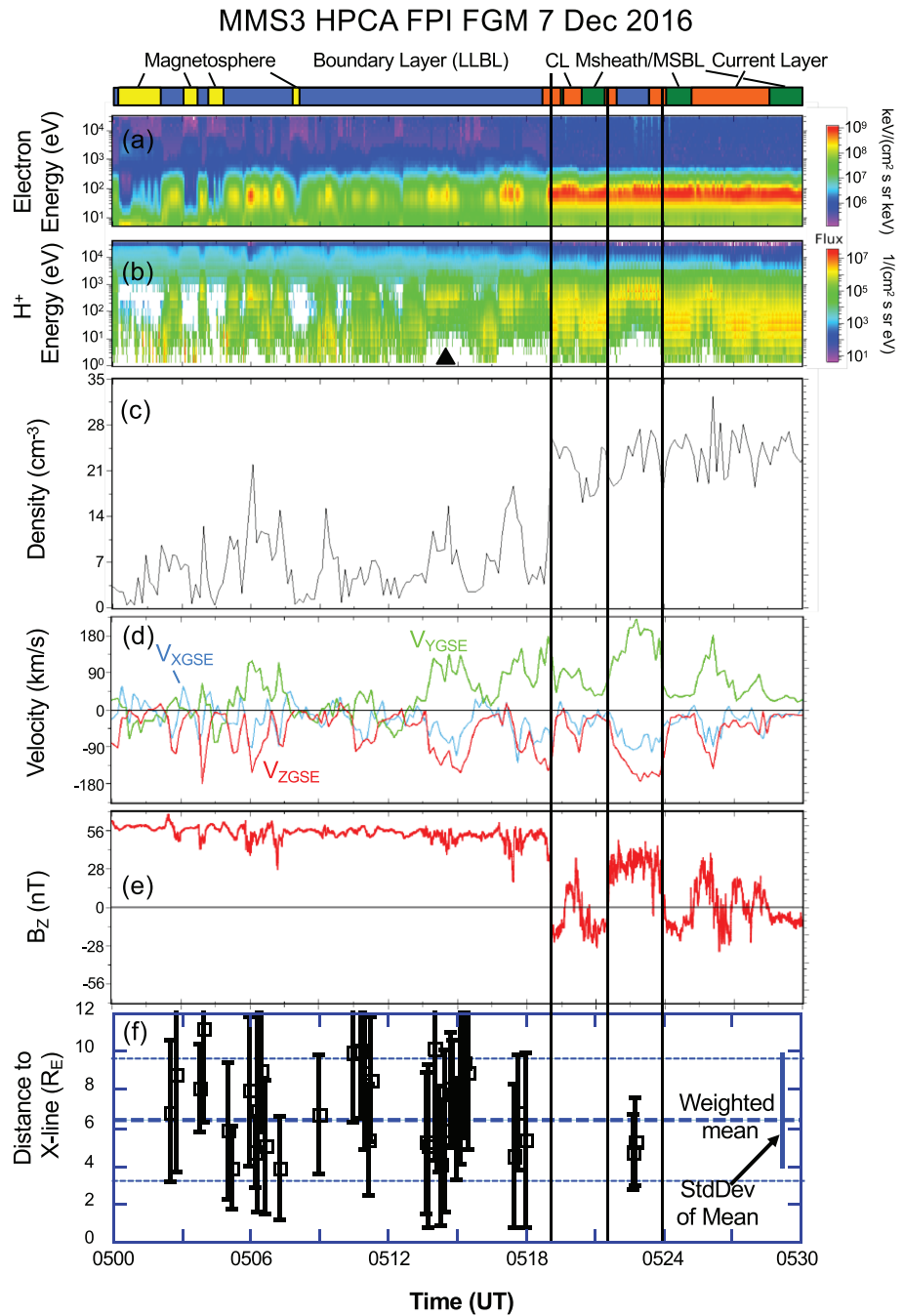


Figure 2. 30 min of data surrounding several magnetopause crossings near the subsolar point. (panels a through e): The omni-directional electron flux, the omni-directional H^+ flux, the H^+ density, the H^+ velocity, B_{ZGSM} , and the computed distance from the spacecraft to the X-line. The black vertical lines show the location of complete magnetopause crossings, and the black triangle in panel (b) shows the time of a 3-D velocity distribution in Figure 3. The spacecraft goes in and out of the low-latitude boundary layer (LLBL) over a 24-min time interval from 0500 UT to 0524 UT. Every time it is in the LLBL, the computed distance from the spacecraft to the X-line remains within $6.8 \pm 3 R_E$. That is, the X-line is quasi-stationary, fluctuating around a more or less fixed distance from the spacecraft, but never moving in a consistent fashion away (or toward) the spacecraft.

Figure 2 shows 30 min of data from MMS3 for magnetopause crossings under conditions similar to those discussed in the introduction. Panels (a) through (f) show the omni-directional electron flux, the omni-directional H^+ flux, the H^+ density, the three components of the H^+ velocity, the B_Z component of the

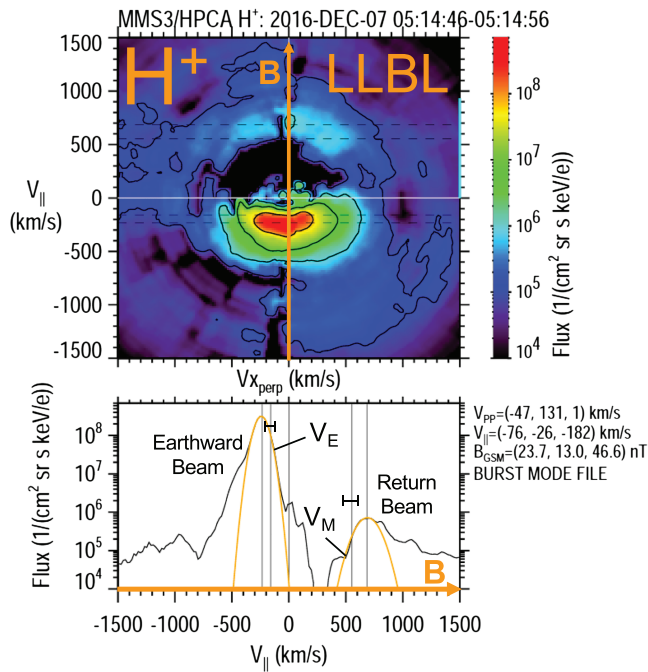


Figure 3. H^+ Velocity distribution in the low-latitude boundary layer (LLBL) from the time period in Figure 2. The $V_{||}$ - V_{\perp} distribution in the top panel is shown in the frame of reference where the velocity perpendicular to the magnetic field is zero. The population propagating antiparallel to the magnetic field at ~ 200 km/s is the magnetosheath population propagating toward the ionosphere. The 1-D cut in this population in the bottom panel is fitted with a Maxwellian and the cutoff velocity is labeled V_E . The population propagating parallel to the magnetic field at ~ 700 km/s is the part of the magnetosheath population that propagated to the ionosphere, mirrored, and returned to the spacecraft. This population is also fit with a Maxwellian and the cutoff velocity is labeled V_M . The cutoff velocities of the earthward and mirrored populations are used to calculate the distance from the spacecraft to the reconnection site.

on the lower-velocity half of the population. The uncertainty in the cutoff velocity is defined as half the velocity difference between the peak and the cutoff velocity.

The second population is very cold and at near-zero parallel velocity. It is the low-energy magnetospheric ion population. This population is also seen in the magnetosphere in Figure 2 at for example, 0501:30 UT in panel (2b). In the boundary layer, for example, at the black triangle in Figure 2 in panel (2b), this population has gained energy in the direction perpendicular to the magnetic field and is no longer at low energy in the spacecraft frame.

The third population is the high-energy ring current. This population has low fluxes, is nearly isotropic, and extends from $|V| > 700$ km/s in Figure 2. This population was on closed field lines in the magnetosphere but is now on open field lines in the LLBL.

The fourth population is the return beam, propagating parallel to the magnetic field at a velocity of about 700 km/s. These ions entered the LLBL along open field lines, propagated antiparallel to the magnetic field to the ionosphere, mirrored, and returned to the spacecraft parallel to the magnetic field. Like the earthward propagating magnetosheath population, the perpendicular temperature of this population is also much larger than the parallel temperature. This population is also fit with a Maxwellian in the bottom panel and the low-speed cutoff is labeled V_M . The higher velocity part of this population merges with the ring current population. However, the fluxes of this return beam are about the same as the fluxes in the magnetosheath H^+ population antiparallel to the magnetic field at the same energy and these fluxes are about a factor of 5 higher than the ring current population at parallel velocities < 800 km/s.

magnetic field in GSM coordinates, and the distance to the X-line calculated from Equation (1). The three nearly complete magnetopause crossings are identified by solid vertical lines and there are several partial crossings in between and after the three crossings that are not identified. Finally, there is a regional identifier bar above panel (a).

The spacecraft starts in the magnetosphere, spends nearly 20 min entering and exiting the LLBL from the magnetosphere. During this 20-min interval, the solar wind IMF clock angle varied by only $\pm 5^\circ$. MMS3 crosses the magnetopause first at 0519 UT, where the B_Z component rotates from positive to negative, and then crosses the boundary two more times after that, before ending up in the magnetosheath at the end of the time period. The multiple intervals in the LLBL, where the density is intermediate between the magnetosheath and magnetospheric densities and the H^+ V_Z velocities are negative and very high, are used here to determine the distance to the reconnection site over ~ 24 min.

Figure 3 shows a detailed H^+ velocity space distribution from the LLBL interval marked by the triangle in the omni-directional H^+ flux in panel (2b). The 2-D cut in the 3-D velocity distribution in Figure 3 is in the frame where the flow velocity perpendicular to the magnetic field (both averaged over 10 s) is zero. Below the 2-D cut is a 1-D cut parallel to the magnetic field along $V_{\perp} = 0$.

The 2-D cut contains four populations. The first population has the highest flux and is propagating antiparallel to the magnetic field. It is responsible for the $-V_Z$, high-speed flows in Figure 2d. This is the magnetosheath population that entered the LLBL along reconnected field lines. The perpendicular temperature of this population is considerably larger than the parallel temperature and the population has a low-speed cutoff.

The antiparallel propagating population is fit with a Maxwellian in the bottom panel and the low-speed cutoff is labeled V_E . The cutoff velocity was determined using a previous process (Fuselier et al., 2000; Trattner et al., 2007a, 2007b), whereby the population is fitted with a Maxwellian and cutoff velocity is defined to be at a flux level that is $1/e$ from the peak

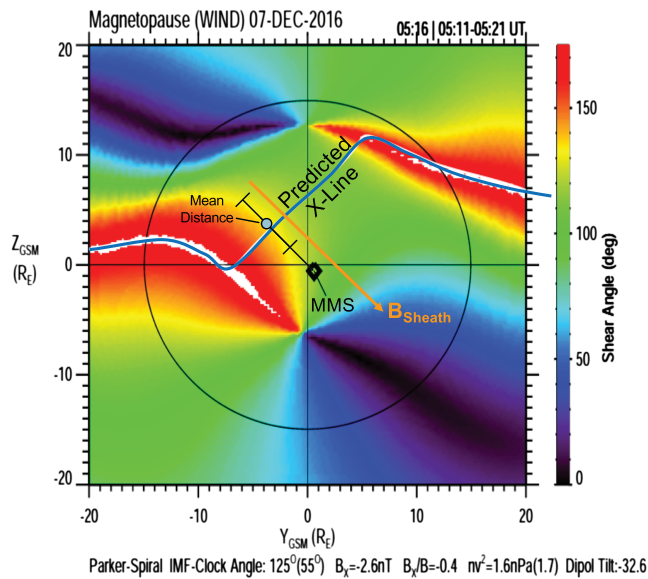


Figure 4. Modeled magnetic shear angle at the magnetopause projected into the Y - Z_{GSM} plane for the time interval in Figure 2. The interplanetary magnetic field conditions that were used to produce this shear angle map are shown at the bottom. Red regions in the map show high magnetic shear and violet regions show low magnetic shear. The blue line shows the location of the X -line predicted by the maximum shear model. The mean distance from the Magnetospheric Multiscale spacecraft to the X -line, determined from the ion populations in the low-latitude boundary layer, is shown by the grey dot. The predicted and observed distances are consistent with one another.

The distance from the spacecraft to the reconnection site is computed from (1) using $|V_E| = 160 \pm 38$ km/s, $|V_M| = 535 \pm 56$ km/s, and $X_M = 9.45 R_E$. As defined above, the uncertainties in the velocities are one half of the velocity between the peak and $1/e$ of the peak. The distance from the spacecraft to the ionosphere along the magnetic field was determined from the Tsyganenko magnetic field model and the spacecraft location. With these numbers and uncertainties, the distance from the spacecraft to the reconnection site for the 10 s time period in Figure 3 was $8 \pm 3 R_E$. The relatively large uncertainty in the distance is due to relatively large uncertainties in the cutoff velocities. Nonetheless, (1) yields the best estimates of the distance when the spacecraft is approximately half-way between the reconnection site and the mirror point, as it is in the example in Figure 3. When the spacecraft is very close to the ionospheric mirror point and relatively far away from the reconnection site, $|V_E| \sim |V_M|$ and the denominator in (1) approaches zero with very large uncertainties. When the spacecraft is very close to the reconnection site and relatively far away from the ionospheric mirror point, $|V_E| \ll |V_M|$ and there are insufficient fluxes of magnetosheath ions at high velocities to determine $|V_M|$. Equivalently, under these conditions, there are insufficient number of magnetosheath ions that have high enough velocity to propagate to the ionosphere and return before the reconnected field line convects past the spacecraft. This is the usual condition at the magnetopause for spacecraft crossings near the subsolar point, except under the special, near-solstice conditions for the event in Figure 3 and outlined in the introduction. The ability to observe a return beam thus depends on the convection speed of the reconnected field line and the distances from the reconnection X -line and the mirror point. These are the quantities that determine if the convection speed of the reconnected field line is “slow enough”.

The velocity distribution in Figure 3 is representative of velocity distributions observed in the LLBL from 0500 to 0524 UT in Figure 2. None of the populations in the LLBL exhibit the characteristics described above that indicate that the spacecraft is far from or close to the reconnection site. The bottom panel in Figure 2 shows the calculated distance to the reconnection site for all of the 10-s LLBL distributions observed by MMS3/HPCA. There are relatively large uncertainties in the distance. However, taken as a group, they show that the reconnection site never moves consistently away from the spacecraft over the 24 min of observations in the LLBL. Assuming that the reconnection site distance is simply fluctuating around a fixed location, the weighted mean of the reconnection distances is $6.8 \pm 3 R_E$. This distance and uncertainty are shown by the blue dashed lines in the bottom panel in Figure 2.

Figure 4 shows how this mean distance to the reconnection X -line is related to the predicted location of the X -line from the maximum shear model. Plotted in Figure 4 are the model magnetic shear angles between the draped magnetosheath and magnetospheric fields on the magnetopause surface. The view is from the Sun and the shear angles are projected into the Y - Z_{GSM} plane. The black circle is the terminator. The maximum shear model predicts the reconnection X -line extends from beyond the dawn terminator along the ridge of magnetic shear angles = 180° (i.e., antiparallel reconnection). The X -line cuts across the dayside magnetopause well above the subsolar point and connects with the antiparallel ridge on the duskside. The observed mean distance to the reconnection site is $6.3 \pm 3 R_E$ and, within the uncertainties, this mean distance is consistent with the location of the predicted X -line.

4. Observations: 29 December 2016 Magnetopause Crossings

The MMS3 spacecraft crossed the magnetopause twice on 29 December 2016 at approximately 0358:30 UT and 0403:45 UT. The spacecraft was close to the subsolar point, but not as close as with the 7 December 2016 event in section 3. The IMF clock angle was 96° and B_x was nearly 0. During the time interval in Figure 5, the solar wind IMF clock angle varied by only $\pm 5^\circ$.

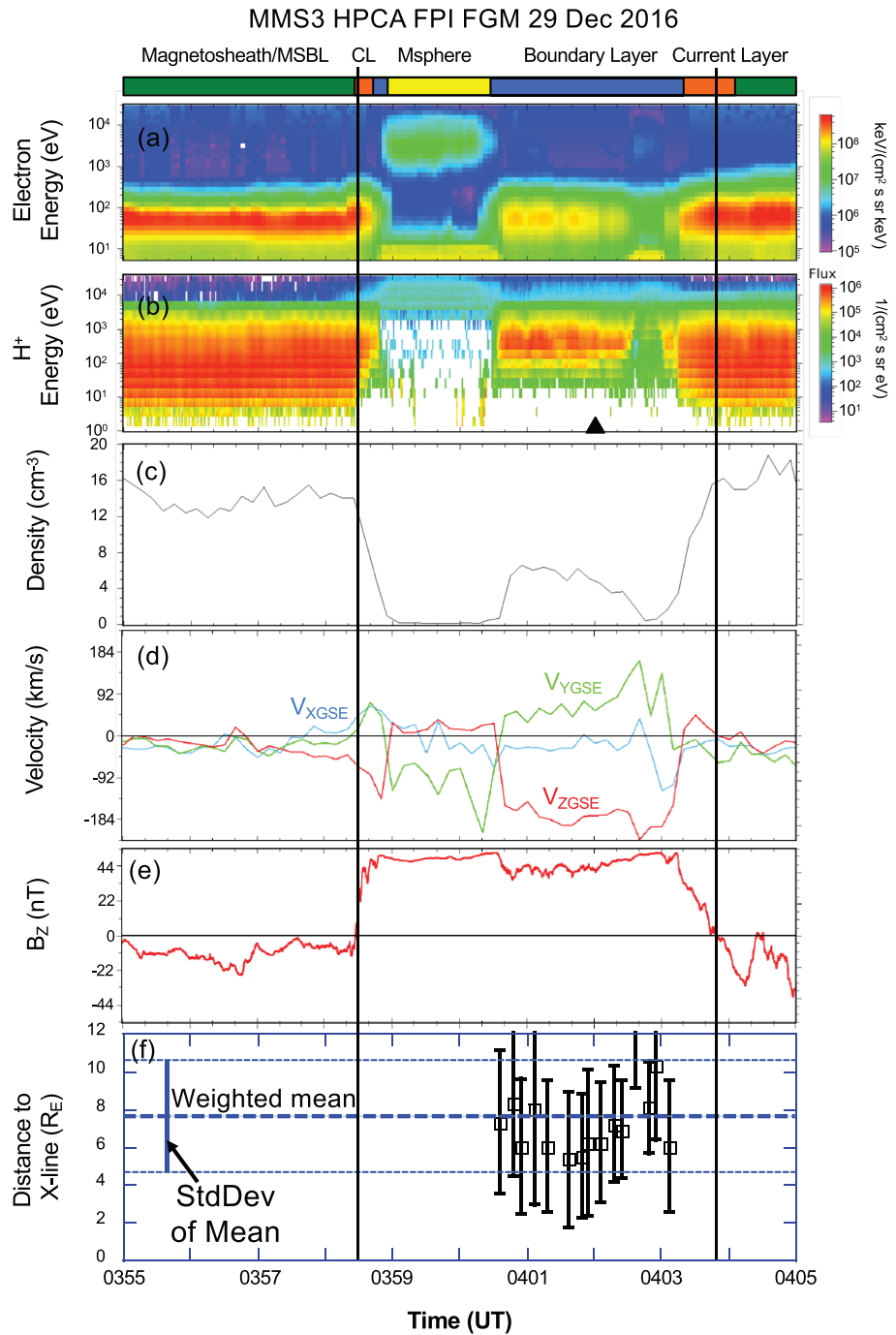


Figure 5. 10 min of data surrounding two magnetopause crossings relatively near the subsolar point. The format and panel identification are the same as in Figure 2. The black vertical lines show the location of complete magnetopause crossings and the black triangle in panel (b) shows the time of a 3-D velocity distribution in Figure 6. The spacecraft crosses the magnetopause at 0358:30 UT and spends a brief time in the magnetosphere. From 0400:30 UT it is continuously in the low-latitude boundary layer. While in the low-latitude boundary layer, the computed distance from the spacecraft to the X-line remains within $7.8 \pm 3 R_E$. That is, the X-line is quasi-stationary, fluctuating around a more or less fixed distance from the spacecraft, but never moving in a consistent fashion away (or toward) the spacecraft.

Figure 5 shows 10 min of data from MMS3 for the two magnetopause crossings. The conditions were similar to the crossings in Figure 2 and the format is the same as in Figure 2. The two complete magnetopause crossings are identified by solid vertical lines. The first crossing at 0358:30 UT from the magnetosheath to

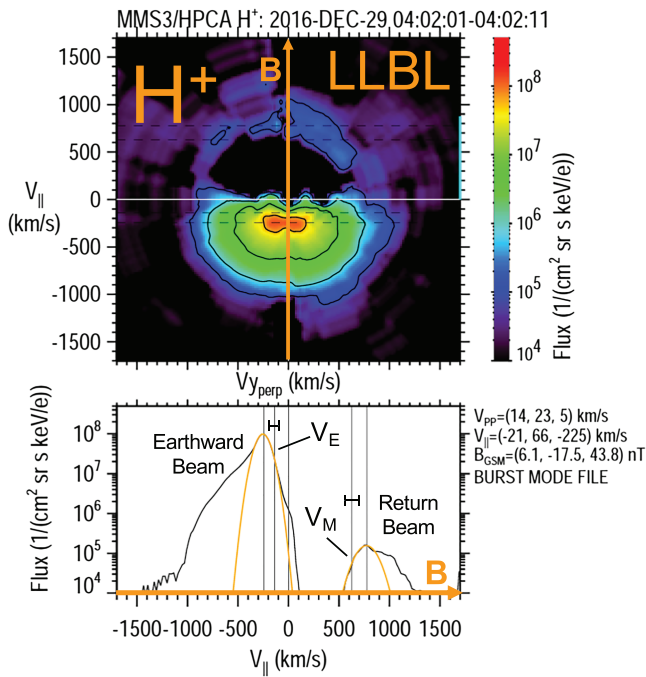


Figure 6. H^+ Velocity distribution in the low-latitude boundary layer (LLBL) from the time period in Figure 5. The format is the same as in Figure 3. The population propagating antiparallel to the magnetic field at ~ 250 km/s is the magnetosheath population propagating toward the ionosphere. The 1-D cut in this population in the bottom panel is fitted with a Maxwellian and the cutoff velocity is labeled V_E . The population propagating parallel to the magnetic field at ~ 800 km/s is the part of the magnetosheath population that propagated to the ionosphere, mirrored, and returned to the spacecraft. This population is also fit with a Maxwellian and the cutoff velocity is labeled V_M . The cutoff velocities of the earthward and mirrored populations are used to calculate the distance from the spacecraft to the reconnection site.

away from the spacecraft with a weighted mean distance of $7.8 \pm 3 R_E$ and is at a more or less fixed distance from the spacecraft.

The location of the X-line relative to the spacecraft and the predicted X-line are shown in Figure 7. The format is the same as Figure 4. In this event, the predicted X-line and the measured mean distance agree within 1σ of one another. However, Trattner et al. (2018) showed that the reconnection X-line often deviates sooner from the antiparallel ridge running from past the dawn terminator at $Z_{GSM} = -4 R_E$ in Figure 7. If the event in Figure 7 is one of these types of events, then the predicted X-line would be closer to the dawn terminator at $Z_{GSM} = 0$ and the predicted and measured distances would be closer than 1σ of one another. These details notwithstanding, Figures 5 and 7, show that MMS3 was quite far from a quasi-stationary X-line.

5. Interpretation

5.1. Single X-line

When the IMF is southward and $|\pm B_Y| \geq |-B_Z|$, the maximum shear reconnection model predicts a single, component reconnection X-line that stretches across the dayside magnetopause at approximately a 45° angle with respect to the $Y-Z_{GSM}$ plane. Around the solstices, this component X-line is still at approximately the same angle with respect to the $Y-Z_{GSM}$ plane, but the line does not pass through the subsolar point. Instead, it crosses the noon meridian in the at $Z_{GSM} \sim 5$ to $10 R_E$ for the winter solstice and $Z_{GSM} \sim -5$ to $-10 R_E$ for the summer solstice. The location of this component X-line near the winter solstice for these IMF conditions is shown schematically in Figure 1 and for two specific events in Figures 4 and 7. Figures 1, 4, and 7, are for IMF $+B_Y$ conditions. For IMF $-B_Y$ conditions, the component reconnection

the magnetosphere is rapid, the boundary is thin, and the interval in the boundary layer is too short for HPCA to make a complete measurement. The spacecraft spends approximately one and a half minutes in the magnetosphere. The magnetosphere is characterized by high energy electrons and protons in panels (5a) and (5b). It then transitions into a nearly 3-min-long LLBL interval. It crosses the magnetopause at 0403:45 UT and reenters the magnetosheath at the end of the interval in Figure 5.

The black triangle in Figure 5 shows the time when the H^+ distribution in the LLBL in Figure 6 was measured. This distribution is representative of the other LLBL distributions observed from 0400:30 UT to 0403 UT. The format is the same as that of Figure 3. In Figure 6, the antiparallel propagating population is the magnetosheath population that entered the LLBL on open field lines and is propagating toward the ionosphere. This population is responsible for the large, negative V_Z velocity in Figure 5c. The ring current population is at velocities greater than about 1200 km/s and has very low density in this event. There is a clear return beam from the ionosphere propagating parallel to the magnetic field. Similar to the populations in Figure 3, the earthward and return beams are fit with Maxwellians and the two cutoff velocities, V_E and V_M , are labeled in the bottom panel of Figure 6.

The distance from the spacecraft to the reconnection site is computed from (1) using $|V_E| = 138 \pm 64$ km/s, $|V_M| = 626 \pm 95$ km/s, and $X_M = 11.06 R_E$. As in the event in section 3, the distance from the spacecraft to the ionosphere was determined from the Tsyganenko 1990 magnetic field model and the spacecraft location. Using (1) and these numbers and uncertainties, the distance from the spacecraft to the reconnection site for the 10-s time period in Figure 5 was $6.2 \pm 4 R_E$.

The distances to the reconnection site computed from all of the measured 3-D distributions in the LLBL interval are shown in the panel (5e) in Figure 5. Although the LLBL interval is considerably shorter than the one in Figure 2, the result is similar. That is, the reconnection site is far

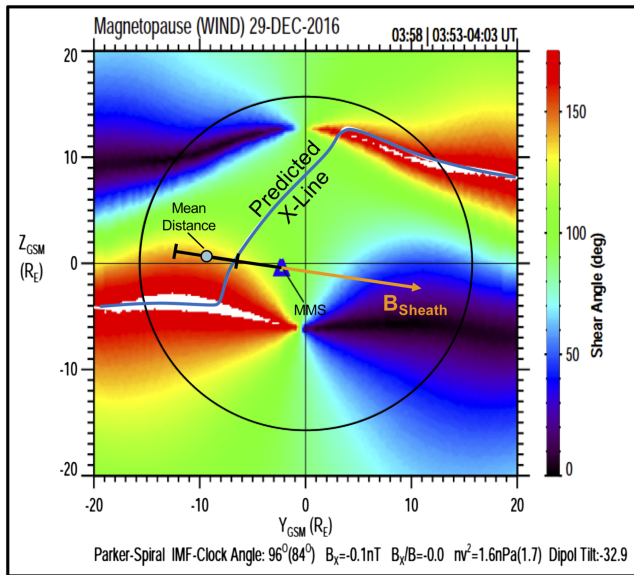


Figure 7. Modeled magnetic shear angle at the magnetopause projected into the Y - Z_{GSM} plane for the time interval in Figure 5. The format is the same as in Figure 4. The mean distance from the MMS spacecraft to the X-line, determined from the ion populations in the low-latitude boundary layer, is shown by the grey dot. The predicted and observed distances are within 1σ of one another.

line is mirrored about the noon meridian. Under the conditions in Figures 4 and 7, a large fraction of the component reconnection X-line may be in a region where the bulk flow speed is super-Alfvénic in the magnetosheath adjacent to the magnetopause and this flow is perpendicular to the reconnection X-line. These high flow speeds raise the question of whether the reconnection X-line, once formed, will remain stationary or will move tailward with the magnetosheath or near the Alfvén speed.

One interpretation for the two events presented in Figures 2, 3, and 4 and 5, 6, and 7 is that there is a primary X-line formed at approximately the predicted distance from the spacecraft. Furthermore, the X-line remains quasi-stationary for long periods of time (i.e., a minimum of several minutes) even though the X-line is in a region where the magnetosheath flow is perpendicular to the X-line and the flow is super-Alfvénic. For the second event (Figures 5, 6, and 7), the Alfvén speed at the spacecraft was ~ 110 km/s and the flow speed in the magnetosheath at the predicted reconnection X-line location, from the gas dynamic model (Spreiter & Stahara, 1985), was ~ 1.35 times the Alfvén speed. If the X-line was moving downward and tailward at this Alfvén speed, then in the ~ 3 min of observations of the X-line location in Figure 5, the distance from the spacecraft to the X-line should have increased by $\sim 4 R_E$. If the X-line was moving at the magnetosheath speed, then the distance from the spacecraft to the X-line should have increased by $\sim 5.4 R_E$.

The contrast between the observed distance to the X-line and its possible motion is much more dramatic for the first event (Figures 2, 3, and 4). For this event, the Alfvén speed was ~ 230 km/s at the spacecraft and the flow speed in the magnetosheath was ~ 1.35 times the Alfvén speed at the location of the X-line. If the X-line were moving downward and tailward at this higher Alfvén speed, then in the ~ 24 min of observation of the X-line location in Figure 2, the distance from the spacecraft to the X-line should have increased by $\sim 63 R_E$. At this distance, MMS3 would have observed that $V_M \sim V_E$ (i.e., the spacecraft was close to the ionospheric mirror point and very far from the reconnection X-line). There were no LLBL distributions that showed these cutoff velocities.

The interpretation of a single, quasi-stationary X-line has some limitations. First, the use of the entering and return beams to calculate the distance to the X-line requires restrictive conditions. As such, there are few MMS observations where the spacecraft is at the subsolar magnetopause near the December solstice and the IMF clock angle is steady with $|\pm B_Y| \geq |-B_Z|$. Thus, the results from the two events presented here are likely to be representative of the other times under the same conditions; however, identifying more events is problematic.

5.2. Multiple X-Lines

The interpretation of the single, primary X-line described in the section 5.1 is not unique. In particular the observations described here do not rule out multiple X-lines at the magnetopause. However, these observations place important constraints on the formation and motion of additional X-lines.

The first important constraint is that secondary X-lines do not form southward of the spacecraft location and those that form northward of the spacecraft do not propagate southward such that they pass over the spacecraft. If either of these conditions were to occur, then counter-streaming ion populations (one from each reconnection X-line) with nearly equal fluxes would be observed in the LLBL. No such distributions were observed in these two events.

There is a second important constraint on the formation and propagation of X-lines northward (away from) the spacecraft. Consider the following scenario: The primary X-line forms at the predicted location and moves northward/tailward. A short time later, a new X-line forms in the original location and moves in the same direction. The combination of the first and second X-lines produces a flux transfer event (FTE).

This scenario is essentially the same as that described by Raeder (2006, 2009) and Hasegawa et al. (2010). In particular, Hasegawa et al. (2010) show observational evidence of multiple X-lines from an event with large dipole tilt and their Figure 2 is a pictorial representation of the formation and motion of the FTE described above. In addition to these simulations and observations, Pu et al. (2005) reported multiple flux ropes at the high latitude northern cusp for a January 2001 event (i.e., near the winter solstice) during a southward IMF interval. Wang et al. (2007) reported an FTE propagating on the flank magnetopause at northern latitudes in a January 2005 event (also near the winter solstice) during an interval when the IMF was southward and had a large B_Y component. Finally, Wilder et al. (2014) reported a tailward retreating X-line at high latitudes during an event when the IMF was northward and they also reported the formation of a new X-line equatorward of the retreating one. While all of these observations and simulations suggest the formation of multiple X-lines, none of them confirm that the primary X-line reforms in the same position as the one that retreats northward/tailward. However, this must happen if this scenario is to be consistent with the observations in Figures 2 and 5.

The observations in this paper also place constraints on the size of the FTE that is formed by the sequential creation of two X-lines. If the time period between the formation of the first X-line, its tailward propagation, and formation of the second X-line is short enough, then the computed distance from the spacecraft to the reconnection X-line will remain within one standard deviation of the mean in Figures 2 and 5. The time between formation, propagation, and formation of the second X-line is limited to approximately the time that the X-line moves 1σ (or $3R_E$). For the second event, the X-line moving at 150 km/s (1.35 times the 110 km/s Alfvén speed) would propagate $3R_E$ in 2 minutes. Thus, the maximum reformation time is 2 minutes and the maximum distance between the two X-lines is $3R_E$. It is probably a coincidence that the estimated size of the FTE reported by Hasegawa et al. (2010) is also $\sim 3R_E$. However, the similarities in the size estimates from very different techniques suggests that FTEs may have a maximum size of a few R_E at the dayside magnetopause.

6. Final Conclusions

Although it is argued here that the X-line remains quasi-stationary or rapidly reforms in the same location, the unanswered question is why this should be the case. For the single X-line interpretation, one possibility is that the component reconnection line does not exist in isolation. As Figures 4 and 7 show, the maximum shear model predicts that the X-line is continuous, stretching from beyond the dawn terminator to beyond the dusk terminator. In particular, the component part of the X-line is linked to the antiparallel parts on the flanks of the magnetopause. It may be that the component part of the X-line cannot move tailward and away from the subsolar point because this motion would require significant changes in the location of antiparallel parts of the X-line. There may be similar constraints on the southward motion of multiple X-lines at the magnetopause.

Acknowledgments

Solar wind data were obtained from the CDAWeb. IDL routines for display of MMS data are also publicly available in the current SPEDAS software package, which is found through the MMS Science Data Center and through the THEMIS TDAS website at <http://themis.ssl.berkeley.edu/software.shtml>. Research at Southwest Research Institute was funded by the NASA MMS prime contract NNG04EB99C. Research at LMATC is under contract 499935Q. Work at IRAP was supported by CNRS and CNES.

References

- Burch, J. L., Torbert, R. B., Phan, T. D., Chen, L. J., Moore, T. E., Ergun, R. E., et al. (2016). Electron-scale measurements of magnetic reconnection in space. *Science*, 352(6290), id.aaf2939. <https://doi.org/10.1126/science.aaf2939>
- Cassak, P. A., Genestreti, K. J., Burch, J. L., Phan, T.-D., Shay, M. A., Swisdak, M., et al. (2017). The effect of a guide field on local energy conversion during asymmetric magnetic reconnection: Particle-in-cell simulations. *Journal of Geophysical Research: Space Physics*, 122, 11,523–11,542. <https://doi.org/10.1002/2017JA024555>
- Dunlop, M. W., Zhang, Q. H., Bogdanova, Y. V., Trattner, K. J., Pu, Z., Hasegawa, H., et al. (2011). Magnetopause reconnection across wide local time. *Annales de Geophysique*, 29(9), 1683–1697. <https://doi.org/10.5194/angeo-29-1683-2011>
- Fuselier, S. A., Frey, H. U., Trattner, K. J., Mende, S. B., & Burch, J. L. (2002). Cusp aurora dependence on interplanetary magnetic field Bz. *Journal of Geophysical Research*, 107(A7), 1111. <https://doi.org/10.1029/2001JA900165>
- Fuselier, S. A., Klumpar, D. M., & Shelley, E. G. (1992). Counter-streaming magnetosheath ions in the dayside low latitude boundary layer. *Geophysical Research Letters*, 19, 425–428.
- Fuselier, S. A., & Lewis, W. (2011). Properties of near-Earth magnetic reconnection from in-situ observations. *Space Science Reviews*, 160, 95–121. <https://doi.org/10.1007/s11214-011-9820-x>
- Fuselier, S. A., Lewis, W. S., Schiff, C., Ergun, R., Burch, J. L., Petrinc, S. M., & Trattner, K. J. (2016). Magnetospheric Multiscale science mission profile and operations. *Space Science Reviews*, 199(1–4), 77–103.
- Fuselier, S. A., Petrinc, S. M., & Trattner, K. J. (2000). Stability of the high-latitude reconnection site for steady northward IMF. *Geophysical Research Letters*, 27, 473–476.
- Fuselier, S. A., Trattner, K. J., & Petrinc, S. M. (2011). Antiparallel and component reconnection at the dayside magnetopause. *Journal of Geophysical Research*, 116, A10227. <https://doi.org/10.1029/2011JA016888>
- Gosling, J. T., Thomsen, M. F., Bame, S. J., Elphic, R. C., & Russell, C. T. (1990). Plasma flow reversals at the dayside magnetopause and the origin of asymmetric polar cap convection. *Journal of Geophysical Research*, 95, 8073–8084.

- Hasegawa, H., Wang, J., Dunlop, M. W., Pu, Z. Y., Zhang, Q. H., Lavraud, B., et al. (2010). Evidence for a flux transfer event generated by multiple X-line reconnection at the magnetopause. *Geophysical Research Letters*, *37*, L16101. <https://doi.org/10.1029/2010GL044219>
- Hesse, M. (2006). Dissipation in magnetic reconnection with a guide magnetic field. *Physics of Plasmas*, *13*, 1220107.
- Lavraud, B., Zhang, Y. C., Vernisse, Y., Gershman, D. J., Dorelli, J., Cassak, P. A., et al. (2016). Currents and associated electron scattering and bouncing near the diffusion region at the Earth's magnetopause. *Geophysical Research Letters*, *43*, 3042–3050. <https://doi.org/10.1002/2016GL068359>
- Lepping, R. P., Acuña, M. H., Burlaga, L. F., Farrell, W. M., Slavin, J. A., Schatten, K. H., et al. (1995). The wind magnetic field instrument. In C. T. Russell (Ed.), *The Global Geospace Mission* (pp. 207–229). Dordrecht, Netherlands: Kluwer Acad.
- Ogilvie, K. W., Chornay, D. J., Fritzenreiter, R. J., Hunsaker, F., Keller, J., Lobell, J., et al. (1995). SWE: A comprehensive plasma instrument for the Wind spacecraft. In C. T. Russell (Ed.), *The Global Geospace Mission* (pp. 55–77). Norwell, Mass: Kluwer Acad.
- Onsager, T. G., & Fuselier, S. A. (1994). The location of magnetic reconnection for northward and southward interplanetary magnetic field. In J. L. Burch, & J. H. Waite, Jr. (Eds.), *Solar System Plasmas in Space and Time, Geophys. Monogr. Ser.*, (Vol. 84, pp. 183–197). Washington DC: American Geophysical Union.
- Onsager, T. G., Thomsen, M. F., Gosling, J. T., & Bame, S. J. (1990). Electron distributions in the plasma sheet boundary layer: Time-of-flight effects. *Geophysical Research Letters*, *17*, 1837.
- Petrinec, S. M., Burch, J. L., Fuselier, S. A., Gomez, R. G., Lewis, W., Trattner, K. J., et al. (2016). Comparison of Magnetospheric Multiscale ion jet signatures with predicted reconnection site locations at the magnetopause. *Geophysical Research Letters*, *43*, 5997–6004. <https://doi.org/10.1002/2016GL069626>
- Petrinec, S. M., Dayeh, M. A., Funsten, H. O., Fuselier, S. A., Heirtzler, D., Janzen, P., et al. (2011). Neutral atom imaging of the magnetospheric cusps. *Journal of Geophysical Research*, *116*, A07203. <https://doi.org/10.1029/2010JA016357>
- Petrinec, S. M., & Fuselier, S. A. (2003). On continuous versus discontinuous neutral lines at the dayside magnetopause for southward interplanetary magnetic field. *Geophysical Research Letters*, *30*(10), 1519. <https://doi.org/10.1029/2002GL016565>
- Petrinec, S. M., Trattner, K. J., & Fuselier, S. A. (2003). Steady reconnection during intervals of northward IMF: Implications for magnetosheath properties. *Journal of Geophysical Research*, *108*(A12), 1458. <https://doi.org/10.1029/2003JA009979>
- Phan, T. D., Kistler, L. M., Klecker, B., Haerendel, G., Paschmann, G., Sonnerup, B. U. Ö., et al. (2000). Extended magnetic reconnection at the Earth's magnetopause from detection of bi-directional jets. *Nature*, *404*(6780), 848–850. <https://doi.org/10.1038/35009050>
- Phillips, J. L., Bame, S. J., Elphic, R. C., Gosling, J. T., Thomsen, M. F., & Onsager, T. G. (1993). Well-resolved observations by ISEE-2 of ion dispersion in the magnetospheric cusp. *Journal of Geophysical Research*, *98*, 13,429–13,440.
- Pollock, C., Moore, T., Jacques, A., Burch, J., Gliese, U., Saito, Y., et al. (2016). Fast plasma investigation for Magnetospheric Multiscale. *Space Science Reviews*, *199*(1–4), 331–406. <https://doi.org/10.1007/s11214-016-0245-4>
- Pritchard, K. R., Burch, J. L., Fuselier, S. A., Webster, J. M., Torbert, R. B., Argall, M. R., et al. (2019). Energy conversion and electron acceleration in the magnetopause reconnection diffusion region. *Geophysical Research Letters*, *46*, 10,274–10,282. <https://doi.org/10.1029/2019GL084636>
- Pu, Z. Y., Wang, J., Dunlop, M. W., Zhang, X. G., Wei, Y., Zhou, X. Z., et al. (2005). Cluster and TC1 five point observations of an FTE on Jan. 4, 2005: A preliminary study. In *Proceedings of the Cluster and Double Star Symposium – 5th Anniversary of Cluster in Space*, ESA SP-598.
- Raeder, J. (2006). Flux Transfer Events: 1. generation mechanism for strong southward IMF. *Annales de Geophysique*, *24*, 381–392.
- Raeder, J. (2009). FTE generation for predominantly east-west IMF, Eos Trans. AGU, 90(52), Fall Meet. Suppl., Abstract SM31A-1516.
- Russell, C. T., Anderson, B. J., Baumjohann, W., Bromund, K. R., Dearborn, D., Fischer, D., et al. (2016). The Magnetospheric Multiscale magnetometers. *Space Science Reviews*, *199*(1–4), 189–256. <https://doi.org/10.1007/s11214-014-0057-3>
- Spreiter, J. R., & Stahara, S. S. (1985). Magnetohydrodynamic and gasdynamic theories for planetary bow waves. In B. T. Tsurutani, & R. G. Stone (Eds.), *Collisionless shocks in the Heliosphere: Reviews of Current Research, Geophys. Monogr. Ser.*, (Vol. 35, p. 85–107). Washington DC: American Geophysical Union.
- Trattner, K. J., Burch, J. L., Cassak, P. A., Ergun, R., Eriksson, S., Fuselier, S. A., et al. (2018). The transition between antiparallel and component magnetic reconnection at Earth's dayside magnetopause. *Journal of Geophysical Research: Space Physics*, *123*, 10,177–10,188. <https://doi.org/10.1029/2018JA026081>
- Trattner, K. J., Burch, J. L., Ergun, R., Eriksson, S., Fuselier, S. A., Giles, B. L., et al. (2017). The MMS dayside magnetic reconnection locations during phase 1 and their relation to the predictions of the maximum magnetic shear model. *Journal of Geophysical Research: Space Physics*, *122*, 11,991–12,005. <https://doi.org/10.1002/2017JA024488>
- Trattner, K. J., Mulcock, J. S., Petrinec, S. M., & Fuselier, S. A. (2007a). Location of the reconnection line at the magnetopause during southward IMF conditions. *Geophysical Research Letters*, *34*, L03108. <https://doi.org/10.1029/2006GL028397>
- Trattner, K. J., Mulcock, J. S., Petrinec, S. M., & Fuselier, S. A. (2007b). Probing the boundary between antiparallel and component reconnection during southward interplanetary magnetic field conditions. *Journal of Geophysical Research*, *112*, A08210. <https://doi.org/10.1029/2007JA012270>
- Trattner, K. J., Petrinec, S. M., Fuselier, S. A., Omid, N., & Sibeck, D. G. (2012). Evidence of multiple reconnection lines at the magnetopause from cusp observations. *Journal of Geophysical Research*, *117*, A01213. <https://doi.org/10.1029/2011JA017080>
- Tsyganenko, N. A. (1995). Modeling the Earth's magnetospheric magnetic field confined within a realistic magnetopause. *Journal of Geophysical Research*, *100*, 5599–5612.
- Vines, S. K., Fuselier, S. A., Petrinec, S. M., Trattner, K. J., & Allen, R. C. (2017). Occurrence frequency and location of magnetic islands at the dayside magnetopause. *Journal of Geophysical Research: Space Physics*, *122*, 4138–4155. <https://doi.org/10.1002/2016JA023524>
- Wang, J., Dunlop, M. W., Pu, Z. Y., Zhou, X. Z., Zhang, X. G., Wei, Y., et al. (2007). TC1 and Cluster observation of an FTE on 4 January 2005: A close conjunction. *Geophysical Research Letters*, *34*, L03106. <https://doi.org/10.1029/2006GL028241>
- Wilder, F. D., Eriksson, S., Trattner, K. J., Cassak, P. A., Fuselier, S. A., & Lybekk, B. (2014). Observation of a retreating x line and magnetic islands poleward of the cusp during northward interplanetary magnetic field conditions. *Journal of Geophysical Research: Space Physics*, *119*, 9643–9657. <https://doi.org/10.1002/2014JA020453>
- Young, D. T., Burch, J. L., Gomez, R. G., de Los Santos, A., Miller, G. P., Wilson, P., et al. (2016). Hot Plasma Composition Analyzer for the Magnetospheric Multiscale mission. *Space Science Reviews*, *199*(1–4), 407–470. <https://doi.org/10.1007/s11214-014-0119-6>